Check for updates

Received: 9 June 2022 | Revised: 16 August 2022 | Accepted: 3 September 2022

DOI: 10.1002/app.53157

RESEARCH ARTICLE

Applied Polymer SCIENCE WILEY

Lightning strike damage resistance of carbon-fiber composites with nanocarbon-modified epoxy matrices

Sotirios Kopsidas[1] | **Ganiu B. Olowojoba**[1] | **Chris Stone**[2] | **David Clark**[2] | **A. Manu Haddad**[2] | **Anthony J. Kinloch**[1] | **Ambrose C. Taylor**[1]

[1]Department of Mechanical Engineering, Imperial College London, London, UK

[2]Morgan-Botti Lightning Laboratory, School of Engineering, Cardiff University, Cardiff, UK

Correspondence
Sotirios Kopsidas, Department of Mechanical Engineering, Imperial College London, London SW7 2AZ, UK.
Email: s.kopsidas15@alumni.imperial.ac.uk

Funding information
UK Engineering and Physical Sciences Research Council (EPSRC), Grant/Award Number: EP/K016792/1

Abstract

Carbon-fiber reinforced polymer (CFRP) composites are replacing metal alloys in aerospace structures, but they can be vulnerable to lightning strike damage if not adequately protected due to the poor electrical conductivity of the polymeric matrix. In the present work, to improve the conductivity of the CFRP, two electrically conductive epoxy formulations were developed via the addition of 0.5 wt% of graphene nanoplatelets (GNPs) and a hybrid of 0.5 wt% of GNPs/carbon nanotubes (CNTs) at an 8:2 mass ratio. Unidirectional CFRP laminates were manufactured using resin-infusion under flexible tooling (RIFT) and wet lay-up (WL) processes, and subjected to simulated lightning strike tests. The electrical performance of the RIFT plates was far superior to that of the WL plates, independent of matrix modification, due to their greater carbon-fiber volume fraction. The GNP-modified panel made using RIFT demonstrated an electrical conductivity value of 8 S/cm. After the lightning strike test, the CFRP panel remains largely unaffected as no perforation occurs. Damage is limited to matrix degradation within the top ply at the point of impact and localized charring of the surface. The GNP-modified panel showed a comparable level of resistance against lightning damage with the existing copper mesh technology, offering at the same time a 20% reduction in the structural weight. This indicates a feasible route to improve the lightning strike damage resistance of carbon-fiber composites without the addition of extra weight, hence reducing fuel consumption but not safety.

KEYWORDS
conducting polymers, graphene and fullerenes, nanotubes, thermosets

1 | INTRODUCTION

Fiber composites comprising continuous fibers embedded in a polymer matrix find extensive use in applications because of their low weight, high mechanical strength, and high stiffness compared to the unmodified polymer.[1] High performance applications commonly use carbon fibers in a thermoset epoxy matrix. As such, carbon-fiber reinforced polymer (CFRP) composites are being increasingly employed in the aerospace industry to replace

This is an open access article under the terms of the Creative Commons Attribution License, which permits use, distribution and reproduction in any medium, provided the original work is properly cited.
© 2022 The Authors. *Journal of Applied Polymer Science* published by Wiley Periodicals LLC.

10974628, 2022, 46, Downloaded from https://onlinelibrary.wiley.com/doi/10.1002/app.53157 by Imperial College London, Wiley Online Library on [29/11/2022]. See the Terms and Conditions (https://onlinelibrary.wiley.com/terms-and-conditions) on Wiley Online Library for rules of use; OA articles are governed by the applicable Creative Commons License

traditional metal alloys, with the most notable examples being the Airbus A350 XWB and Boeing 787 aircraft, which consist of up to 50% of composites by weight.[2] Nevertheless, fiber-composite aircraft structures are inherently vulnerable to damage by lightning strike due to their inferior and non-homogeneous electrical conductivity compared to metallic equivalents. Lightning strikes are a common concern for aircraft, statistically striking each aircraft once per 1,000 to 10,000-flight hours, which is on average once a year for a commercial plane.[3] Aircraft structures traditionally made of aluminum and titanium alloys have been used safely for many years, since they offer protection to the aircraft in the event of a lightning strike by conducting the current and allowing it to flow through the skin of the aircraft. Consequently, aircraft parts made of composites require lightning strike protection (LSP), with the most widespread practice involving the bonding of a metal mesh or foil onto the outer surface of the composite structure. The metal protection is made of either copper (Cu) or aluminum (Al) due to their high specific electric conductivity (i.e., the ratio of electrical conductivity to density). However, this addition of a metal mesh or foil results in an undesirable increase in the total structural weight of the aircraft, thus reducing the weight- and fuel-savings associated with the use of composite materials.[3] Another disadvantage associated with the use of Cu and Al meshes bonded onto CFRP surfaces is their dissimilarity, with carbon fibers being nobler than the two metals, with the outcome being galvanic corrosion and a subsequent reduction in the electrical conductivity of the corroded metal-mesh interface areas.[4]

To overcome the above limitation of the existing metallic mesh or foil LSP strategy, research has focused on alternative materials that are both lightweight and conductive. In this respect, carbon nanomaterials are viewed as excellent candidates, due to their intrinsically high electrical conductivity and low density. For example, carbon nanotubes (CNTs) have a density of 1.7 g/cm^3,[5] compared to 8.9 g/cm^3 for copper.[3] One approach has used carbon nanomaterials in the form of highly conductive films and coatings, adhered to the surface of composites. For example, Han et al.[6] developed a novel LSP coating composed of a 70 μm thick carbon nanotube film laid on top of an insulating hexagonal boron nitride (h-BN) modified adhesive, which had previously been coated onto the CFRP laminate. The CNT film-coated laminate demonstrated a greatly improved resistance to lightning strike damage, compared to the pristine uncoated laminate when subjected to a test lightning current of 40 kA. Similarly, Xia et al.[7] reported the fabrication of a silver modified CNT film protecting the CFRP structure and observed that the residual compressive strength of the CNT film-protected composite was greater than that of the Cu mesh-protected composite after being subjected to a lightning strike test. In another study, the preparation of a reduced graphene oxide (RGO) enriched CFRP surface, resulted in an increase in the surface conductivity of the composite from 16 S/cm (for the pristine CFRP) to 440 S/cm, which led to a drastic improvement in the resistance to lightning damage compared to the unmodified laminate.[8] Rajesh et al.[9] studied different conductive coatings for LSP and concluded that expanded copper foil (ECF) co-cured with the CFRP substrate, which is the currently applied industry solution, is the superior approach in restricting the lightning damage. The authors measured a sheet resistance of approximately 5×10^{-3} Ω/m for the panel, although to acquire a more accurate value this needs to be converted to a surface conductivity by multiplying with the mesh thickness. Although the authors only provide the areal weight of the mesh, which is 200 g/m^2, assuming a base metal thickness of 0.076 mm, which is typical for a mesh of such weight,[10] a surface conductivity of 2.5×10^4 S/cm is obtained.

An alternative approach to improve the lightning strike damage resistance of composite structures has focused on the enhancement of the electrical conductivity of the insulating thermoset matrix. Hirano et al.[11,12] have demonstrated that the conductivity of the matrix in CFRPs has a significant influence on the effectiveness of lightning damage suppression. These authors replaced the epoxy matrix with an intrinsically conductive thermoset based on polyaniline (PANI). The electrical conductivity was measured to be 148 and 0.74 S/cm for the in-plane and out-of-plane directions, representing a respective six and 27 times increase in comparison to the conventional carbon fiber (CF)/epoxy composite.[12,13] This translated into a superior damage suppression capability for the CF/PANI composites compared to their epoxy matrix counterparts for lightning current tests of 40 kA.[12]

Nonetheless, conductive polymers are typically very difficult to process due to their very high viscosity and, consequently, do not currently represent a viable option for the development of conductive fiber-reinforced composites on an industrial scale. The same applies for solutions using carbon-rich coatings and films as these are impossible to scale up, as well as extremely difficult to repair in an event of a strike. However, the addition of a nanocarbon filler to the epoxy matrix can increase its electrical conductivity,[14] as well as its stiffness and fracture properties,[15,16] whilst retaining good processability. Several authors have reported that the modification of epoxies with carbon nanofillers results in CFRP

10974628, 2022, 46, Downloaded from https://onlinelibrary.wiley.com/doi/10.1002/app.53157 by Imperial College London, Wiley Online Library on [29/11/2022]. See the Terms and Conditions (https://onlinelibrary.wiley.com/terms-and-conditions) on Wiley Online Library for rules of use; OA articles are governed by the applicable Creative Commons License

composites with enhanced electrical and thermal properties.[17–19] Additionally, there are a few studies which investigate the effect of such nanofillers in polymer matrices and the subsequent lighting strike damage tolerance of the resulting CFRP composites.[20–23]

In the present study, the lightning strike damage resistance of conventional unidirectional (UD) CF/epoxy composites is improved by the incorporation of graphene nanoplatelets (GNPs) and CNTs into the epoxy matrix. The GNPs consist of more than 10 graphene layers but do not exceed a thickness of 100 nm,[24] so are an ultra-thin form of graphite and represent one of the most commercially-available sources of graphene. The modified epoxy resin was integrated into the CFs using either a resin-infusion under flexible tooling (RIFT) or a wet lay-up (WL) manufacturing process prior to curing. The manufactured composites were subjected to test lightning currents of waveform D to evaluate their resistance to lightning strike damage. The resulting damage was visually evaluated and characterized using ultrasonic inspection. The electrical conductivities of the composites were measured before and after the strike. The impact of the manufacturing process and the nanocarbon-modification of the epoxy matrix on the damage resistance to laboratory-generated lightning strikes are discussed. This innovative analysis of these multiscale composites will allow the lightning strike tolerance of lightweight composite structures to be further optimized.

2 | MATERIALS AND MANUFACTURING

2.1 | Materials

Epoxy is the most common matrix for CFRP, so an anhydride-cured epoxy polymer was used. A diglycidyl ether of bisphenol-A (DGEBA) liquid epoxy resin (Araldite LY556; Huntsman, UK) with an epoxide equivalent weight (EEW) of 185 g/eq was cured using an accelerated methylhexahydrophthalic acid anhydride (Albidur HE600; Evonik, Germany) with an anhydride equivalent weight (AEW) of 170 g/eq. The cured epoxy has a glass transition temperature (T_g) of 159°C,[25] as measured by dynamic mechanical thermal analysis (DMTA). Graphene nanoplatelets (GNPs) with an average lateral size of 4.5 μm, average platelet thickness of 12 nm and surface area of 80 m^2/g (Grade AO-3; Graphene Supermarket, USA) were used. These were selected as they produced the most electrically-conductive epoxies in trials using a range of commercially-available GNPs. Multiwalled carbon nanotubes (MWCNTs) with an average length of 1.5 μm, average diameter of 9.5 nm and surface area of 250–300 m^2/g (NC7000; Nanocyl, Belgium) were used. Unidirectional (UD) stitched carbon-fiber (CF) fabric (UT-C400; Gurit, UK) with an area weight of 400 g/m^2 and a tow number of 12,000; and a Cu mesh with a weight of 73 g/m^2 and an open area of 84% (2Cu[110]4–100 FA; Dexmet Corporation, USA) were used to produce the composites.

2.2 | Preparation of nanocarbon-modified epoxy matrices

The GNPs and CNTs were dispersed into the liquid epoxy resin by stirring using a spatula followed by three-roll milling (3RM). The epoxy/nanocarbon filler mixtures were passed through a three-roll mill (80E; EXAKT, Germany) eight times at a roller speed of 220 rpm and temperature of 40°C. The roller gaps were set to 5 μm. The curing agent was added to the pre-dispersed resin and mixed with a mechanical stirrer (RZR 2012; Heidolph, Germany) fitted with a radial flow impeller at 500 rpm and 60°C for 15 min. The resulting mixture was degassed in a vacuum oven at −1 bar for a minimum of 30 min to remove all the air bubbles. Note that the resulting mixtures were observed to be very stable, with no settling observed over much longer timescales than those required for manufacturing of the CFRP laminates. The nanocarbon-modified epoxy mixtures were either cast into steel molds to produce bulk epoxy plates or infused into the CF fabric to produce carbon-fiber reinforced polymer (CFRP) laminates. For the manufacture of the bulk epoxy plates, the degassed epoxy mixtures were poured into preheated steel molds coated with release agent (Frekote 700NC; Henkel, Germany) and cured for 1 h at 90°C, followed by 2 h at 160°C in a fan oven. The molds were left to cool down slowly to room temperature prior to the cured plates being removed.

2.3 | Manufacturing of carbon-fiber composites

CFRP laminates were manufactured using two different processes: (a) resin infusion under flexible tooling (RIFT), and (b) wet lay-up (WL), see Figure 1. The fiber stack used 8 plies of CF fabric in a UD arrangement, producing cured laminates about 3 mm thick. For laminates manufactured via the RIFT method, the CF fabric was cut into 600 × 360 mm^2 rectangles using a rotary knife (the maximum size possible with the hotplate used); and, for those made via WL, the fabric was cut into 320 × 320 mm^2 squares. The WL laminates were chosen to be smaller to ensure that a high-quality composite

10974628, 2022, 46, Downloaded from https://onlinelibrary.wiley.com/doi/10.1002/app.53157 by Imperial College London, Wiley Online Library on [29/11/2022]. See the Terms and Conditions (https://onlinelibrary.wiley.com/terms-and-conditions) on Wiley Online Library for rules of use; OA articles are governed by the applicable Creative Commons License

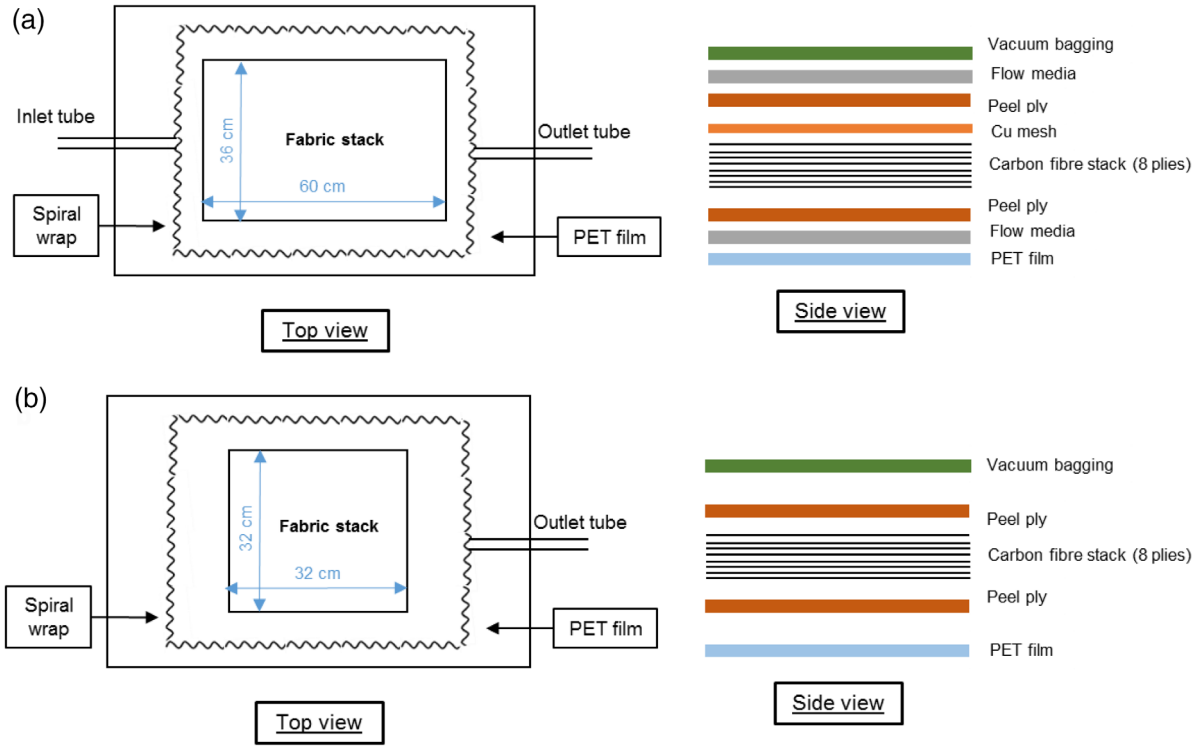


FIGURE 1 Schematic diagram for the fabric arrangement for the (a) resin infusion and (b) wet lay-up processes. [Color figure can be viewed at wileyonlinelibrary.com]

could be produced. A temperature-controlled hotplate (HP1836URS; Wenesco, USA) was used to produce the composite laminates. For the RIFT process, a poly(ethylene terephthalate) (PET) film of 100 μm thickness (Mylar A; UK Insulations, UK) was laid on the hotplate and secured with polyester tape (Flashtape; Cytec, UK). A layer of peel-ply (234 TFP; Tygavac, UK) and flow media (N1031; Newbury Engineered Textiles, UK) were placed at the top and bottom of the CF stack, and the infusion stack was placed on the PET film. The lay-up was sealed using a vacuum bag (VB200; Easy Composites, UK), held down with tacky tape (Vacuum Bagging Gum Sealant Tape; Easy Composites, UK). The outlet of the mold was connected to a vacuum pump through a resin catch pot (ASK2128; Aerovac, UK) using silicone and fluoropolymer tubes (RS Components, UK). The degassed epoxy mixture was infused into the mold through the inlet by applying a vacuum pressure of −1 bar and was allowed to wet the fabric stack until the resin flow reached the outlet. A cure cycle of 90°C for 1 h and 160°C for 2 h was used. For the WL process, PET film was attached to the hotplate and a peel-ply placed on top. A layer of CF was added, resin was spread onto the fibers with a paint roller, and the process repeated for the remaining plies. A layer of peel-ply was added. Spiral wrap (RS Pro Spiral Wrap Polyethylene; RS Components, UK) was placed around the perimeter of the fiber stack to create a uniform vacuum pressure. The lay-up was sealed using a vacuum bag, and the outlet connected to the vacuum pump. The vacuum was applied to remove excess resin from the fabric stack, and the same cure cycle was used. For the Cu mesh-protected laminate, a layer of Cu mesh was placed on top of the CF plies and below the top peel-ply layer, as indicated in Figure 1a, and was cured with the lay-up. The conductivity of the Cu mesh was quoted by the manufacturer as 1.4×10^4 S/cm in the short way of diamond (SWD) and 5.5×10^4 S/cm in the long way of diamond (LWD). An illustration of the mesh geometric properties is provided in the work of Gagne.[3]

3 | CHARACTERIZATION

3.1 | Microscopy studies

Optical microscopy was used to investigate the dispersion of the nanocarbon filler in the modified epoxy matrices of CFRP laminates produced by RIFT. A sample of approximately 25×25 mm^2 was cut from either end of the laminate, corresponding to the inlet and outlet. The samples were mounted in a cold mount epoxy (VariDur; Metprep, UK) and were allowed to cure overnight at room temperature. The mounted samples were ground with a rotary polishing machine (Saphir 520; Metprep,

10974628, 2022, 46, Downloaded from https://onlinelibrary.wiley.com/doi/10.1002/app.53157 by Imperial College London, Wiley Online Library on [29/11/2022]. See the Terms and Conditions (https://onlinelibrary.wiley.com/terms-and-conditions) on Wiley Online Library for rules of use; OA articles are governed by the applicable Creative Commons License

UK) using emery paper from 320 grit to 4000 grit to remove excess cold mount epoxy and generate a flat surface. They were then polished using diamond suspensions from 6 to 0.25 μm to eliminate scratches. Images were taken using an optical microscope (AXIO Scope; Carl Zeiss, Germany).

3.2 | Electrical characterization

Electrical impedance spectroscopy (EIS) was used to measure the electrical conductivity of the bulk epoxy polymers. Samples of $10 \times 10 \times 2$ mm^3 were coated on both surfaces with a conductive silver paint and pressed between two capacitor plates in a two-electrode cell setup using a Reference 600 potentiostat (Gamry Instruments, USA). The tests were conducted inside a Faraday cage to prevent electromagnetic interference, using a root mean square (RMS) alternating voltage of 10 mV over a frequency range from 100 to 1 MHz.

The electrical resistance of the CFRP test panels was measured with a HP3458A multimeter (Hewlett-Packard, USA) using a four-probe arrangement prior to the lightning strike tests. The RIFT laminates were trimmed to 550×340 mm^2 and the WL laminates to 300×300 mm^2 to produce homogeneous edges and ensure secure fixing in the test frame. Holes were drilled around the edges of the test panels, and two metallic screws with electrodes attached were passed through directly opposing holes to measure the electrical resistance in that direction. Two electrical resistance determinations were made for both the longitudinal (i.e., parallel to the fibers) and transverse (i.e., perpendicular to the fibers) directions. The resistance values were converted to conductivity using the test panel dimensions.

3.3 | Simulated lightning current tests

Lightning current tests, replicating Waveform D as specified in SAE ARP5412B,[26] were conducted using the purpose-built impulse current generator at the Morgan-Botti Lightning Laboratory, Cardiff University, UK. The test panels were screwed onto an aluminum adapter, and the test rig was grounded via an earth rod. The lightning current was applied to the center of the test panels, through a copper fuse wire which was tied to the tip of the discharge electrode. The applied impulse current was measured using a Pearson 3880 current monitor (Pearson Electronics, USA) and recorded using an NI PXI5105 Oscilloscope (National Instruments, USA). Waveform D has a peak current amplitude of 100 kA and is used to represent a subsequent return stroke current impulse in multiple-strike lightning. Furthermore, Waveform D is used to certify the vast majority of the airframe, unlike waveform A that is used only for primary attachment points, such as the wing tips, nose or empennage.[27] Strikes of 100 kA are typically used for full-scale structures or subcomponents but are far too high for small-scale tests,[28] so a peak current of 40 kA was applied in the present work as has been used for testing samples of a similar size in the literature.[8] The current waveform is exponential and can be characterized by the current peak value, the time to peak current (t_1) and the time to decay to 50% of its maximum amplitude (t_2).[11,12] A typical measured waveform is shown in Figure 2. The electrical charge (Q) and action integral (AI), which represent the total energy and specific energy of the impulse current, respectively, can be calculated using:[6]

$$Q = \int I\,dt \tag{1}$$

$$\mathrm{AI} = \int I^2\,dt \tag{2}$$

where I is instantaneous current magnitude. The testing conditions for the simulated lightning current tests are shown in Table 1.

3.4 | Monitoring experiment progress and post-test characterization

The experiment was monitored using high-speed (Fastcam SA5; Photron, USA), thermal (SC7750L; FLIR, USA) and still (D700; Nikon, Japan) cameras to investigate the damage suppression behavior of the tested laminates. The test lightning current caused damage in the CFRP in a similar way to impact damage.[28] The temperature versus time response after the strike was obtained from the thermal camera images at 100 frame intervals (i.e., approximately 0.3 s). The highest temperature recorded for each frame corresponds to the temperature at the strike point, with 80°C being the upper limit of detection of the thermal camera. The tested panels were photographed to evaluate the degree of damage. The electrical resistance was measured to determine the effect of the applied lightning impulse current on the electrical properties. Ultrasonic C-scanning was employed to determine the internal damage of the test panels. The test panels were analyzed on the side of the strike using a Prisma portable ultrasonic flaw detector (Sonatest, UK). The detector was equipped with an X3-Glider-Compact Composite Linear Scan phased

10974628, 2022, 46, Downloaded from https://onlinelibrary.wiley.com/doi/10.1002/app.53157 by Imperial College London, Wiley Online Library on [29/11/2022]. See the Terms and Conditions (https://onlinelibrary.wiley.com/terms-and-conditions) on Wiley Online Library for rules of use; OA articles are governed by the applicable Creative Commons License

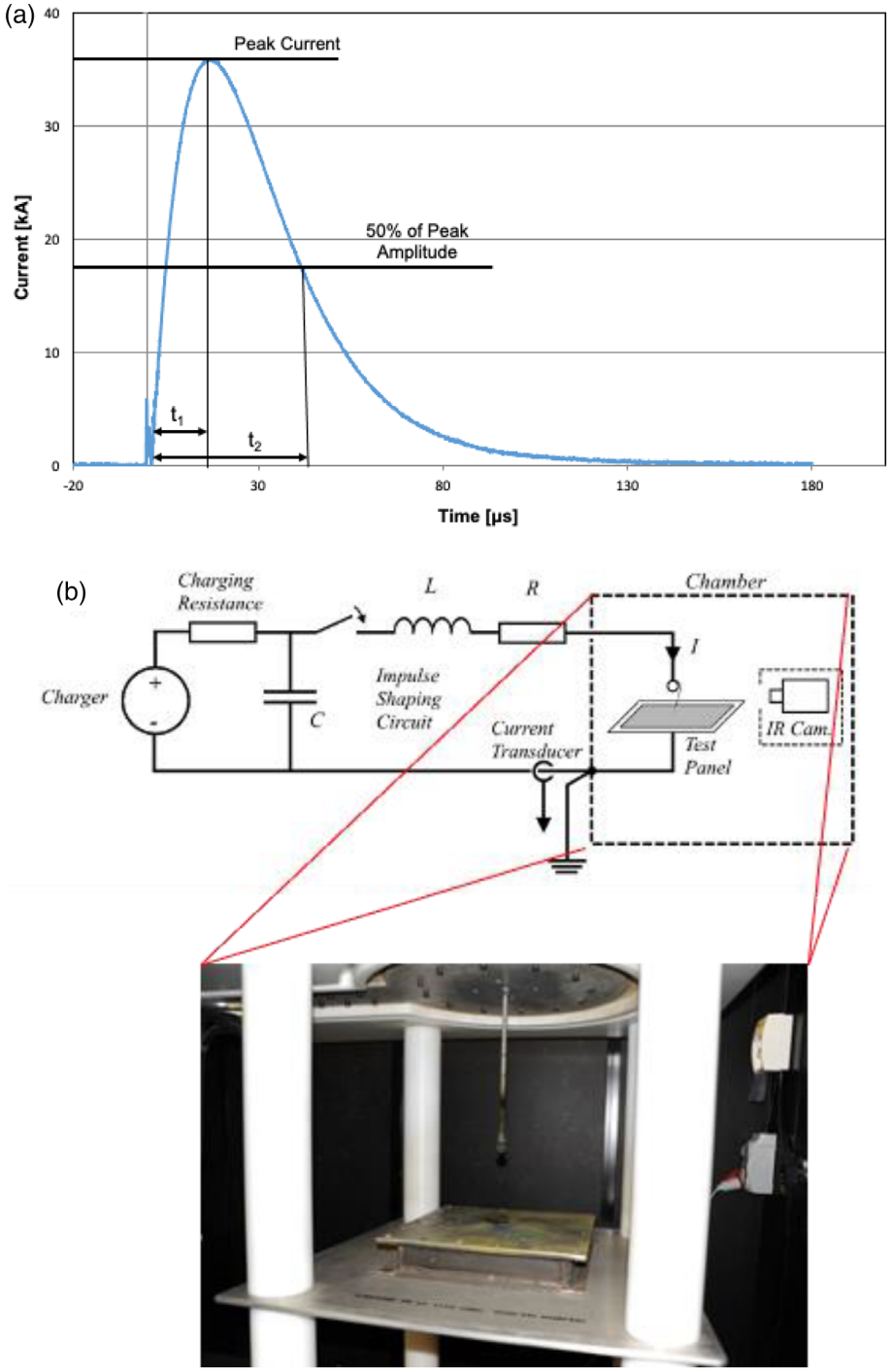


FIGURE 2 (a) Measured simulated lightning current waveform D, with a peak amplitude of 37 kA. (b) Circuit diagram for the lightning strike tests. The insert has a close-up image of the test rig, showing the high-voltage electrode and a metallic test panel set up on the ground electrode. [Color figure can be viewed at wileyonlinelibrary.com]

array transducer, with a frequency of 5 MHz and a 64-element array.

4 | RESULTS AND DISCUSSION

4.1 | Introduction

The electrical conductivities of the nanocarbon-modified epoxy polymers were first measured, and the results were used to select the formulations for the matrices with which the CFRP test panels were manufactured. When CFRP is manufactured using RIFT, there is always a concern that filtering of the nanoparticles can occur and affect the matrix properties, so optical microscopy was employed to examine the extent of filtering. The relative fiber volume fraction between the RIFT and WL panels was calculated, and the electrical conductivity was measured both pre- and post-strike. The temperature distributions measured following the impact of the simulated

10974628, 2022, 46, Downloaded from https://onlinelibrary.wiley.com/doi/10.1002/app.53157 by Imperial College London, Wiley Online Library on [29/11/2022]. See the Terms and Conditions (https://onlinelibrary.wiley.com/terms-and-conditions) on Wiley Online Library for rules of use; OA articles are governed by the applicable Creative Commons License

TABLE 1 Testing conditions for simulated lightning currents.

CFRP panel	Matrix	Manufacturing process	Peak current (kA)	Waveform t_1 (μs)	Waveform t_2 (μs)	Action integral (A^2s)
E-R	Epoxy	RIFT	36.0	16.7	41.1	35,100
G-R	0.5 wt% GNP	RIFT	37.0	16.3	40.4	36,400
GC-R	0.5 wt% GNP/CNT (8:2)	RIFT	35.9	16.4	41.7	35,300
E-W	Epoxy	WL	33.4	21.2	46.3	30,300
G-W	0.5 wt% GNP	WL	33.3	19.9	45.2	30,200
GC-W	0.5 wt% GNP/CNT (8:2)	WL	32.8	18.3	43.0	29,700
E-CM-R	Epoxy/Cu mesh	RIFT	36.1	23.1	46.6	33,800

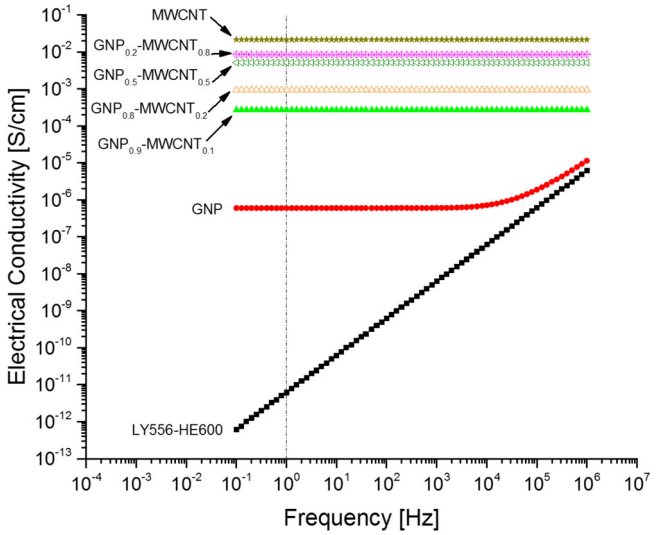


FIGURE 3 Electrical conductivities of the epoxy polymers with varying GNP:CNT ratios at a constant overall concentration of 0.5 wt% of nanocarbon filler. A frequency of 1 Hz is used for comparison as indicated by the dashed line. [Color figure can be viewed at wileyonlinelibrary.com]

lightning strike tests are then presented. Finally, optical characterization of the damage caused by the lightning test current is presented, and the findings are compared to those of ultrasonic examination.

4.2 | Electrical conductivities of the nanocarbon-modified epoxy polymers

Electrically conductive epoxy polymers were developed by incorporating GNPs and CNTs into the epoxy resin.[25] Figure 3 shows the electrical conductivity versus frequency for the bulk epoxy polymers modified with a fixed nanocarbon filler loading of 0.5 wt%. The amount of nanofiller was selected based on the reported percolation thresholds (p_c) for GNP-modified epoxies prepared via 3RM,[19,29] which range between 0.3 and 1 wt%. The addition of 0.5 wt% of GNPs was found to be sufficient to produce an electrically conductive composite, see Figure 3. Hence, the addition of higher loadings is unnecessary as it will increase the viscosity and compromise the manufacturing process. CNT/epoxy composites demonstrate a significantly lower percolation threshold than their GNP counterparts, with p_c values in the range of 0.0025–0.1 wt%.[30,31] However, the 0.5 wt% loading is kept for consistency amongst all the nanocarbon formulations.

The conductivity of the unmodified epoxy is frequency-dependent, which is characteristic of an insulator.[32] The nanocarbon-modified epoxies are electrically conductive as their conductivity is essentially independent of frequency, see Figure 3. These contain a sufficient amount of nanocarbon to be above the percolation threshold. Addition of 0.5 wt% GNPs resulted in an increase in the electrical conductivity of the matrix by five orders of magnitude at a frequency of 1 Hz, which will be used as the benchmark frequency as is commonly done.[30] For the hybrid GNP/CNT materials, higher fractions of CNTs resulted in higher conductivities, with no synergy being observed.[33] The conductivity increased by more than three orders of magnitude for a CNT mass fraction of 0.2 compared to the GNP-only filled epoxy polymer. Gradually increasing the CNT fraction results in minor conductivity improvements, with a maximum increment of times 30 being recorded when the CNT fraction is raised from 0.1 to 0.8, see Figure 3. However, higher fractions of CNTs are not desirable as they result in higher viscosities for the epoxy matrix that impede processability, which is attributed to the stronger particle-particle and polymer-particle interactions encountered in highly-filled CNT-modified polymers. This is explained mechanistically by the ability of CNTs to readily form a network compared to graphene sheets.[34] Therefore, the nanocarbon-modified matrices selected for the manufacture of the CFRP test panels, were 0.5 wt% GNP and

10974628, 2022, 46, Downloaded from https://onlinelibrary.wiley.com/doi/10.1002/app.53157 by Imperial College London, Wiley Online Library on [29/11/2022]. See the Terms and Conditions (https://onlinelibrary.wiley.com/terms-and-conditions) on Wiley Online Library for rules of use; OA articles are governed by the applicable Creative Commons License

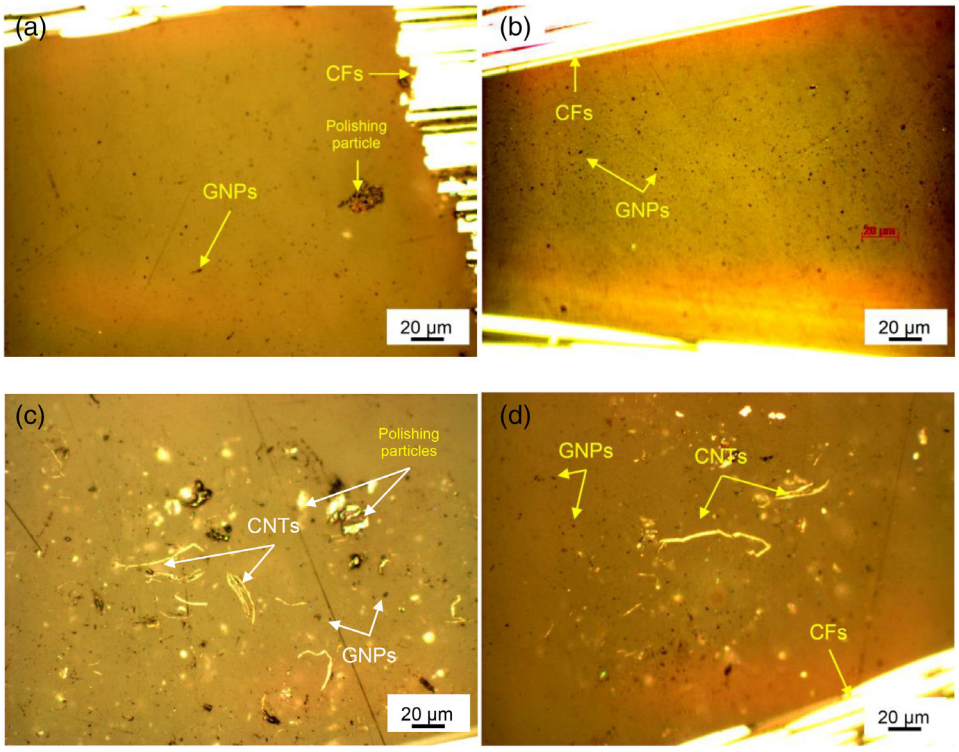


FIGURE 4 Optical microscopy images of the cross-section of CFRP samples produced using RIFT at ×50 magnification: (a) 0.5 wt% GNP at the inlet, (b) 0.5 wt% GNP at the vacuum outlet, (c) 0.5 wt% GNP/CNT (mass ratio 8:2) at the inlet and (d) 0.5 wt% GNP/CNT (8:2) at the vacuum outlet. [Color figure can be viewed at wileyonlinelibrary.com]

0.5 wt% GNP/CNT hybrid at an 8:2 mass ratio, see Table 1, as they offered the best compromise between high electrical conductivity and low viscosity. The values obtained are in excellent agreement with the values reported in the literature. For example, Chandrasekaran et al. for a 0.5 wt% GNP-filled epoxy composite processed via 3RM reported an electrical conductivity value of 10^{-5} S/cm.[29]

4.3 | Dispersion of nanocarbon

Optical microscopy was employed to investigate the dispersion of the nanocarbon filler to determine the extent of filtration during the infusion in the CFRP test panels manufactured using the RIFT process. Nanoparticle filtration has been widely acknowledged to occur during infusion-based processes, such as resin transfer molding (RTM).[35] However, despite filtering effects leading to laminates with a non-uniform filler distribution in the matrix, improvements in the electrical, thermal, and mechanical properties of carbon-fiber composites have still been reported.[17,36–39] Note that, for the CFRP test panels fabricated via the WL process, the distributions of the nanocarbon filler are relatively uniform as the CFs were manually wetted with the modified resin.

Optical microscopy images for the G-R and GC-R CFRP laminates at the inlet and outlet of the infusion are shown in Figure 4. Samples were cut from either edge of the laminates, representing the two extremities of the infusion process, to enable the observation of differences in the optical appearance between the inlet and the outlet, which would indicate the presence of filtering. The CFs appear as bright yellow rods, and the matrix is orange. The graphene agglomerates appear as uniformly distributed black or yellow spots, see Figure 4a,b, and the CNTs as yellow spaghetti-like structures, see Figure 4c,d. The relatively low magnification allows the degree of dispersion to be seen over a large area, whilst the very characteristic shapes of the GNPs and CNTs allow them to be clearly identified. The presence of similar numbers of agglomerates at the inlet and outlet indicates that no significant filtering has occurred. This is also highlighted by the visual inspection of the resin color at the outlet, which is identical to that at the inlet. For heavily filtered systems, it has been previously observed that the resin at the outlet is clear, as all of the filler particles have been filtered out by the fibers during the infusion process.[35]

4.4 | Fiber volume fraction

The electrical properties of CFRP laminates are dependent on the fiber volume fraction (V_F) as the CFs are conductive, so it is necessary to determine the V_F values of the tested laminates. The V_F of the CFRP test panels was calculated based on the following equation according to ASTM D3171[40]:

10974628, 2022, 46, Downloaded from https://onlinelibrary.wiley.com/doi/10.1002/app.53157 by Imperial College London, Wiley Online Library on [29/11/2022]. See the Terms and Conditions (https://onlinelibrary.wiley.com/terms-and-conditions) on Wiley Online Library for rules of use; OA articles are governed by the applicable Creative Commons License

TABLE 2 Mean thicknesses of the CFRP test panels produced via the RIFT and WL processes, and the calculated fiber volume fractions (V_F) based on Equation (3)

	Laminate thickness (h) [mm]		Calculated V_F	
Matrix	**RIFT**	**WL**	**RIFT**	**WL**
Epoxy	2.9	4.1	0.62	0.44
0.5 wt% GNP	2.8	4.6	0.64	0.39
0.5 wt% GNP/CNT (8:2)	2.9	4.5	0.62	0.40

TABLE 3 Electrical conductivity of the CFRP test panels in the longitudinal and transverse directions, before and after the conduct of the simulated lightning strike tests

			Pre-strike		Post-strike	
CFRP panel	**Matrix**	**Manufacturing process**	**Longitudinal (S/cm)**	**Transverse (S/cm)**	**Longitudinal (S/cm)**	**Transverse (S/cm)**
E-R	Epoxy	RIFT	4.9 ± 0.4	0.052 ± 0.000	7.2 ± 0.7	0.072 ± 0.001
G-R	0.5 wt% GNP	RIFT	8.0 ± 0.1	0.074 ± 0.000	9.1 ± 0.2	0.094 ± 0.000
GC-R	0.5 wt% GNP/CNT (8:2)	RIFT	7.2 ± 0.0	0.046 ± 0.000	9.0 ± 0.1	0.065 ± 0.000
E-W	Epoxy	WL	0.10 ± 0.02	0.012 ± 0.000	0.25 ± 0.01	0.022 ± 0.002
G-W	0.5 wt% GNP	WL	0.09 ± 0.05	0.012 ± 0.000	0.27 ± 0.08	0.021 ± 0.001
GC-W	0.5 wt% GNP/CNT (8:2)	WL	0.13 ± 0.00	0.037 ± 0.000	0.27 ± 0.01	0.044 ± 0.001
[a] E-CM-R	Epoxy/Cu mesh	RIFT	—	—	—	—

[a]Values for the E-CM-R panel are not reported, as the obtained values were not consistent due to the existence of the copper mesh on the surface of the laminate.

$$V_F = \frac{A_F \times N}{\rho_F \times h} \quad (3)$$

where A_F is the surface density of the CF fabric (equal to 400 g/m^2), N is the number of plies, ρ_F is the volume density of the CF (taken as 1.79 g/cm^3) and h is the laminate thickness.[18] Since both the RIFT and the WL laminates are composed of eight plies of CF fabric, the difference in the V_F is solely dependent on thickness variation. Table 2 lists the thicknesses of the RIFT and WL laminates along with the calculated V_F values. The WL laminates are about 1 mm thicker than their RIFT counterparts, which means that the RIFT laminates possess a greater CF content by about 40% to 65% compared to that of the WL laminates. The reason for this difference is owed to the fact that more resin is impregnated during the WL process, which cannot be subsequently squeezed out during curing due to the absence of a laminating press.

4.5 | Electrical conductivities of the CFRP laminates

The electrical resistances of the test panels were determined using a four-probe setup. Table 3 presents the electrical conductivity of the CFRP test panels, before and after they were subjected to the simulated lightning strike tests. The RIFT test panels demonstrate almost two orders of magnitude superior electrical conductivity in the longitudinal direction compared to the WL test panels due to the higher V_F of the RIFT test panels. The longitudinal conductivity of UD laminates is heavily dependent on the fiber properties,[17] and since CFs are electrically conductive, the conductivity is dominated by the value of V_F. In the transverse direction, both the RIFT and WL test panels demonstrate a conductivity of the order of 10^{-2} S/cm, indicating that the conductivity is controlled by the conductivity of the matrix. The RIFT test panels show a somewhat higher conductivity than the WL test panels, confirming that any filtering effects associated with the RIFT process must be insignificant. The electrical properties of the two sets of CFRP test panels manufactured by the RIFT or the WL processes can be compared against the respective unmodified matrix as a benchmark. For the pre-strike measurements, the greatest enhancement for the RIFT test panels occurs with the addition of 0.5 wt% GNPs, see Table 3. The electrical conductivity of the G-R panel demonstrates a 63% and 42% improvement in the longitudinal and transverse directions respectively, compared to the unmodified panel (E-R). Despite the fact that the bulk electrical conductivity of the GNP/CNT hybrid (at 8:2 mass ratio) is three orders of magnitude higher than the GNP-only filled

10974628, 2022, 46, Downloaded from https://onlinelibrary.wiley.com/doi/10.1002/app.53157 by Imperial College London, Wiley Online Library on [29/11/2022]. See the Terms and Conditions (https://onlinelibrary.wiley.com/terms-and-conditions) on Wiley Online Library for rules of use; OA articles are governed by the applicable Creative Commons License

epoxy (see Figure 3), the superior electrical conductivity of the hybrid is not transferred to the multiscale composite. This is attributed to the high viscosity of the hybrid-modified blend, which led to poorer infusion of the fabric and a reduced fiber wetting. This explains why the transverse conductivity of the GC-R panel is slightly inferior to that of the E-R panel. The poor processability of the CNT blends is confirmed by the inability to infuse a RIFT laminate using a matrix modified with 0.5 wt% CNTs. In contrast, for the CFRP test panels made using the WL process, the hybrid formulation imparts the best electrical properties, which agrees with the bulk conductivities shown in Figure 3. For the transverse direction in particular, an increment of about 200% in the conductivity (vs. the E-W panel) is observed, see Table 3. This is because during the WL manufacturing process the CF plies are manually impregnated with the resin, which means that this process is relatively unaffected by the higher viscosity of the hybrid-modified epoxy matrix.

The measured electrical conductivity of unmodified CFRP laminates varies considerably between different studies, since there are numerous parameters that will influence the conductivity of the laminates, such as the type of carbon fabric, lay-up, manufacturing process, carbon fiber volume content in the cured laminate as well as the characterization method. For UD carbon/epoxy laminates, conductivity values for the longitudinal direction ranging from 62 to 220 S/cm have been quoted in the literature.[11,17,41] The values reported in the present study for the RIFT-made epoxy laminate (E-R) are approximately one order of magnitude lower, the most likely explanation being a lower carbon fiber volume content arising from the manufacturing method, or differences in the carbon-fiber fabric which will affect the inherent electrical conductivity of the CF fabric, such as carbon-fiber tow or surface composition. The electrical conductivity values reported for the transverse direction range considerably from approximately 0.5 to 0.005 S/cm,[11,17,41] with the value measured in the present study for the E-R panel being in the middle of this range. The increases in the bulk electrical conductivity of the CFRP panel manufactured via RIFT and modified with 0.5 wt% of GNPs (i.e., G-R panel) are very consistent with values reported in the literature. For example, Lin et al.[23] have reported that modification of an epoxy resin with 0.5 and 1 wt% GNPs resulted in a reduction of surface resistance by 56.5% and 51.7%, respectively, compared to the reference unmodified CFRP laminate. Similar to our study, the doubling of the concentration of the conductive filler did not lead to the expected decrease in the surface resistance, with one explanation provided being the higher viscosity of the resin system. In addition, Lampkin et al.[21] reported a decrease of 31% in the surface resistance with addition of CNTs in the epoxy matrix (although the concentration is not mentioned) compared to the unmodified CFRP laminate. This agrees well with our experimental observation that the conductivity improvement capability of CNTs is weaker than that of GNPs in CFRP laminates manufactured via resin-infusion processes.

For the Cu mesh-protected CFRP panel (E-CM-R), the electrical conductivity is not reported in Table 3 due to the difficulties in obtaining a reliable value. The average values recorded were 3.2 S/cm and 13.3 S/cm for the longitudinal and transversal directions, respectively. The individual resistance measurements varied considerably and, in addition, there was a very high fluctuation in the values recorded by the multimeter prior to the final value being displayed. This difficulty in the measurement of electrical resistance can be attributed to the presence of the Cu mesh. The measurement method assumes homogeneity of the sample as it measures the resistance of the bulk and not that of the surface. The Cu mesh acts as an effective short-circuit of the bulk material, where the electrical contact made between the electrodes and Cu mesh is intermittent due to the edge contact. It is difficult to estimate the surface conductivity of the E-CM-R panel since, in theory, it should be inferior to that of the pristine Cu mesh, which is about 10^4 S/cm, see Section 2.3. The Cu mesh is fully impregnated by the resin during the infusion process, which ultimately will have an influence on the electrical conductivity of the Cu. However, for reference purposes, we can utilize the previously deduced value from the work of Rajesh et al.[9] of a surface conductivity in the order of 10^4 S/cm as a representative value for the E-CM-R panel, although the mesh utilized in the study of Rajesh et al. is almost three times heavier than the one used in the present study.

The post-strike electrical conductivities show the same trend as the pre-strike measurements. The electrical conductivity increases following the impact of the lightning current, indicating a change in the internal structure of the panel. It is suggested that this could be an outcome of fiber alignment, with the flowing current straightening the CFs, leading to shorter conduction paths. In addition, in the arc attachment area, that is, the area around the strike location, very high temperatures develop resulting in charring of the epoxy matrix. This occurs typically in the temperature range between 450 and 600°C.[42] Charring leads to a local increase in the conductivity, due to its significantly higher electrical conductivity (i.e., 1 S/cm),[43] which is about 11 orders of magnitude higher compared to that of the original epoxy. Moreover, for test panels which exhibit damage, a likely scenario is for broken fibers to bridge across to adjacent fibers,[44] resulting in the formation of conductive paths local to the

10974628, 2022, 46, Downloaded from https://onlinelibrary.wiley.com/doi/10.1002/app.53157 by Imperial College London, Wiley Online Library on [29/11/2022]. See the Terms and Conditions (https://onlinelibrary.wiley.com/terms-and-conditions) on Wiley Online Library for rules of use; OA articles are governed by the applicable Creative Commons License

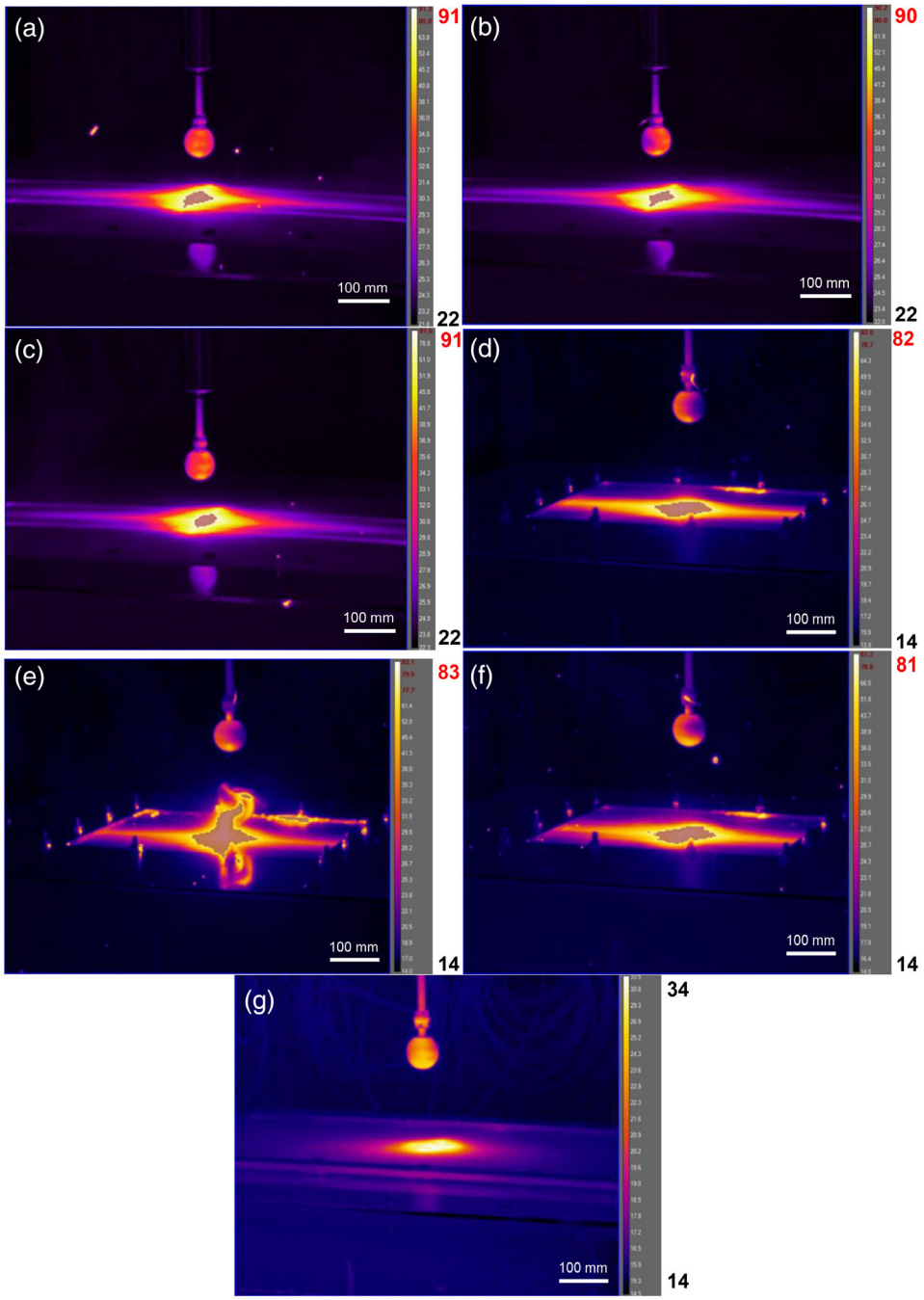


FIGURE 5 Post-strike thermal images showing temperature distribution for the: (a) E-R, (b) G-R, (c) GC-R, (d) E-W, (e) G-W, (f) GC-W and (g) E-CM-R composite test panels at 100 frames (approximately 0.3 s) after the impact of the arc. (Temperature shown in °C, and the red values above 80°C indicate temperatures beyond the camera detection limit.) [Color figure can be viewed at wileyonlinelibrary.com]

strike point, so an electrical current can now travel between the fibers bypassing the far less-conductive epoxy matrix. This increases the overall electrical conductivity of the tested post-strike panel compared to its pre-strike condition.

4.6 | Thermal behavior during the lightning strike tests

The temperature versus time response after the strike was obtained from the thermal camera images to investigate the heat dissipation process. Figure 5 presents the thermal images of the laminates at 100 frames, that is, at approximately 0.3 s, after the impact of the electric arc. For the CFRP test panels made using the RIFT process (without the Cu mesh), see Figure 5a–c, the heat dissipation is oriented predominantly along the fibers, that is, longitudinally, and is visible as purple lines, resembling 'avenues' transferring heat from the extremely hot-strike attachment area, which is colored white in the thermal images, to the cooler edges of the plate. This is expected as the CFs are far more thermally conductive than the matrix, and hence the majority of the heat energy is dissipated in the

10974628, 2022, 46, Downloaded from https://onlinelibrary.wiley.com/doi/10.1002/app.53157 by Imperial College London, Wiley Online Library on [29/11/2022]. See the Terms and Conditions (https://onlinelibrary.wiley.com/terms-and-conditions) on Wiley Online Library for rules of use; OA articles are governed by the applicable Creative Commons License

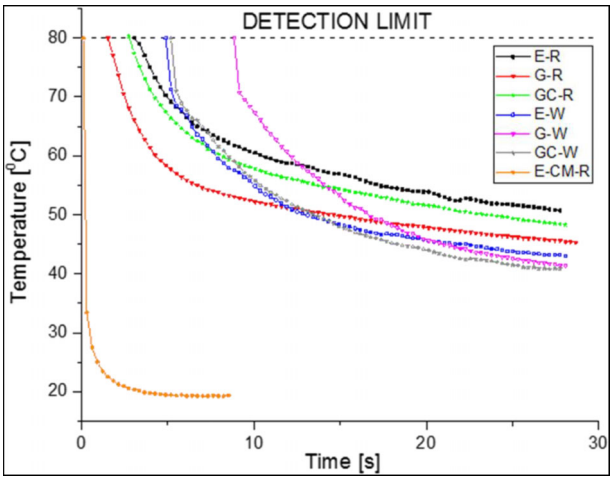


FIGURE 6 Temperature at the strike point against time following the impact of the simulated lightning strike for the CFRP test panels. Temperatures beyond 80°C cannot be detected by the thermal camera. [Color figure can be viewed at wileyonlinelibrary.com]

longitudinal direction. The white regions, which indicate the highest temperatures, extend perpendicular to the fibers as the transverse direction has a lower heat dissipation capacity due to the lower thermal conductivity of the matrix compared to the CF. Exposure of the epoxy matrix to high temperatures will lead to its pyrolysis. Thermogravimetric analysis (TGA) in nitrogen has shown that the epoxy matrix used has a temperature of 5% mass loss ($T_{5\%}$) of 368°C, and thermal decomposition occurs over a temperature range from approximately 350 to 450°C.[25] The temperature in the strike area is plotted against time in Figure 6, showing that the temperature drops to below 80°C between 2 and 3.5 s after the strike. There is no information on the actual temperatures before those times, as the thermal camera has a detection limit of 80°C. No further damage is expected below 80°C, as the cured epoxy has a glass transition temperature (T_g) of 159°C, as measured by dynamic mechanical thermal analysis (DMTA). Thus, the test panels are exposed to the very high temperatures, which may cause damage, for only a very short time.

The heat build-up of the CFRP test panels made using the WL process, see Figure 5d–f, is substantially larger than for the RIFT test panels, see Figure 5a–c. The higher thermal charge is a consequence of higher heat generation after the strike and slower thermal dissipation. The highest temperature, that is, white colored, regions have a rhombus-like shape for the WL test panels, whereas they predominantly extend perpendicular to the fibers for the RIFT test panels. This difference arises because the longitudinal electrical conductivity of the WL test panels is about two orders of magnitude lower than the RIFT test panels, see Table 3. Also, their lower fiber volume fraction results in a reduced thermal conductivity and less effective thermal dissipation. The thermal dissipation process is slower for the WL test panels than for the RIFT test panels, since 5.5 to 9 s is required for the temperature to drop below the detection limit of the camera, see Figure 6.

For the Cu mesh-protected CFRP panel (E-CM-R), which is representative of the existing LSP strategy,[3] the dissipation of heat was uniform, forming a circular temperature distribution around the strike point, see Figure 5g. The heat dissipation is also more rapid than for the other CFRP test panels, with the temperature at the strike area reducing to 34°C at 0.3 s after impact for the E-CM-R panel, see Figure 6. This is to be expected as Cu has a relatively high thermal conductivity and a very high electrical conductivity, which minimizes the Joule heating during the dissipation of the electrical current.[12] Despite the very quick heat dissipation that the Cu mesh is offering, it is still not sufficient to prevent the vaporization of the mesh in the vicinity of the strike area, see Figure 7d. This is due to the very small thickness of the mesh, that is, approximately 0.5 mm thick, which does not allow it to withstand the impact of the electric discharge. Essentially, the Cu mesh acts as a sacrificial layer, preserving the structural integrity of the CFRP by enabling quick dissipation of the lightning strike current.

4.7 | Damage arising from the lightning strike tests

The images of the CFRP test panels made using the RIFT process following the completion of the lightning current tests are presented in Figure 7. The test panel with the unmodified epoxy matrix (E-R) is shown in Figure 7a. The test panel shows a shallow puncture hole at the location of impact which has partly perforated the panel through the thickness. A similar shallow puncture hole appears for the test panel which has a matrix modified with the hybrid nanocarbon filler (GC-R), see Figure 7c. In both instances, the puncture is approximately circular in shape and about 10 mm in diameter, which arises from the pyrolysis of the epoxy matrix. Broken fibers are present in the vicinity of the puncture, but there are no signs of delamination, with only the top ply having been damaged. (Note that attempts to measure the depth of the damage using ultrasonic B-scan were unsuccessful due to signal scattering arising from the waviness of the CFRP surface.)

On the contrary, modification of the matrix with 0.5 wt% GNPs offers protection from lightning strike damage to the composite, as no partial perforation occurs

10974628, 2022, 46, Downloaded from https://onlinelibrary.wiley.com/doi/10.1002/app.53157 by Imperial College London, Wiley Online Library on [29/11/2022]. See the Terms and Conditions (https://onlinelibrary.wiley.com/terms-and-conditions) on Wiley Online Library for rules of use; OA articles are governed by the applicable Creative Commons License

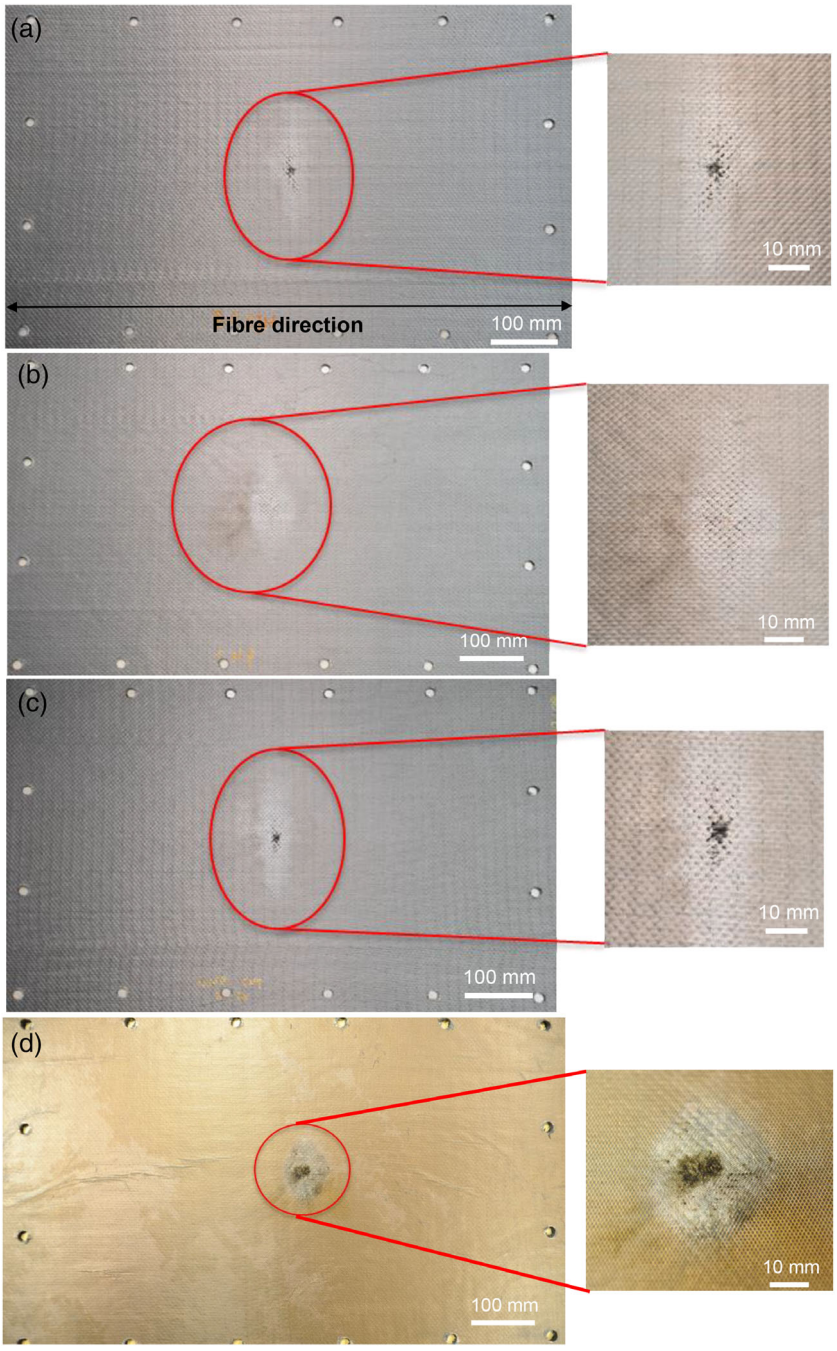


FIGURE 7 Damage of the RIFT CFRP composite test panels subjected to lightning currents of 40 kA: (a) epoxy (E-R), (b) 0.5 wt% GNP (G-R), (c) 0.5 wt% GNP/CNT (GC-R) and (d) epoxy/Cu mesh (E-CM-R). The magnified region provides a close-up of the damaged area. [Color figure can be viewed at wileyonlinelibrary.com]

and the CFRP test panel remains largely unaffected by the lightning test current, see Figure 7b. Damage is limited to matrix degradation at the point of impact and localized charring of the surface. The superior lightning damage suppression is due to the higher electrical conductivity of the G-R test panel compared to the E-R and GC-R test panels, see Table 3.

For the CFRP RIFT test panels without the Cu mesh, as shown in Figure 7a–c, the matrix degraded areas, visible as the faded colored areas in the vicinity of the strike point, extend perpendicularly to the direction of the fibers, that is, from top to bottom in the images. This confirms the observations of the thermal images, where a heat build-up was seen in the transverse direction, as shown in Figure 5a–c.

The CFRP test panel incorporating the Cu mesh (E-CM-R) shows vaporization of the copper mesh around the impact area accompanied by matrix degradation and localized charring of the CFRP surface, see Figure 7d. There is no puncture of the panel by the electric arc. The mesh protects the test plate by distributing the electrical current over the surface, preventing it from entering the

10974628, 2022, 46, Downloaded from https://onlinelibrary.wiley.com/doi/10.1002/app.53157 by Imperial College London, Wiley Online Library on [29/11/2022]. See the Terms and Conditions (https://onlinelibrary.wiley.com/terms-and-conditions) on Wiley Online Library for rules of use; OA articles are governed by the applicable Creative Commons License

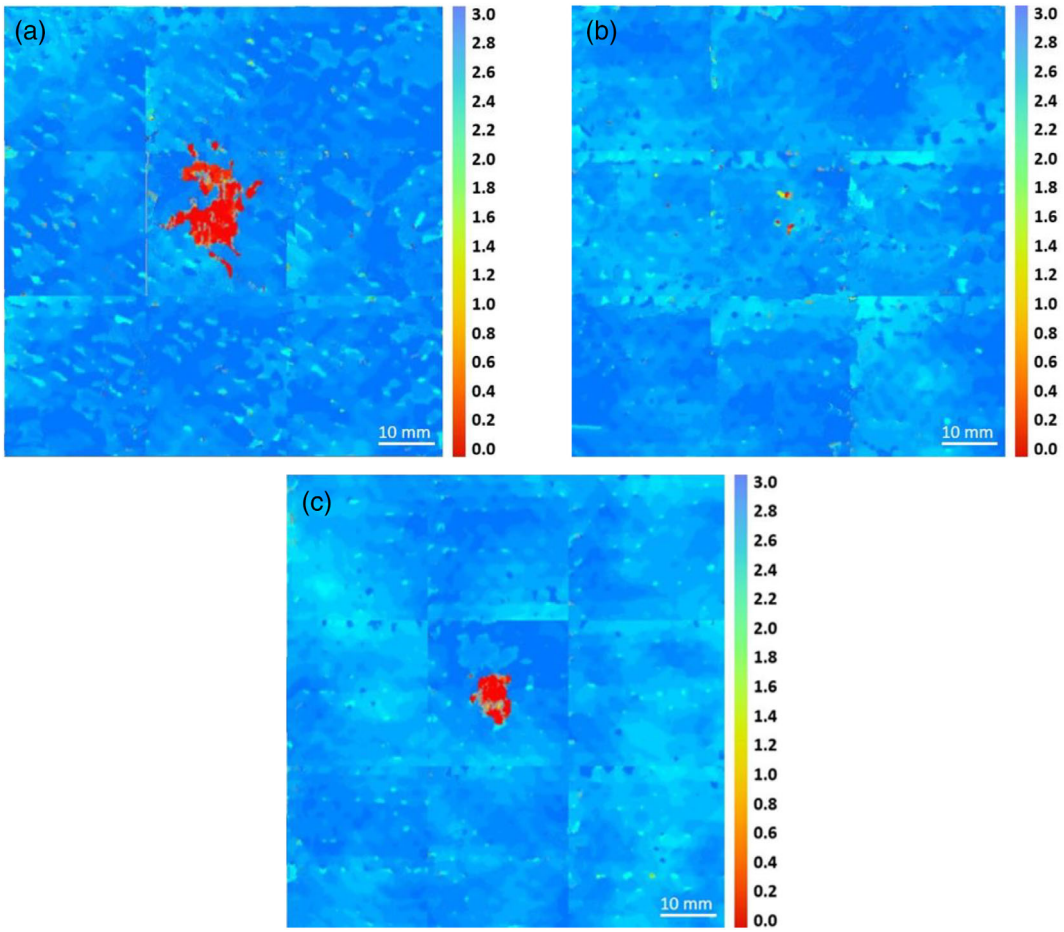


FIGURE 8 C-scans of the RIFT CFRP composite test panels after simulated lightning current tests of 40 kA: (a) epoxy (E-R), (b) 0.5 wt% GNP (G-R), (c) 0.5 wt% GNP/CNT (GC-R). Areas shown in red represent structural damage, while blue indicates non-damaged areas. [Color figure can be viewed at wileyonlinelibrary.com]

CFRP layers in any significant way. The thermal images, shown in Figure 5, indicate that the outer ply of the CFRP acts in the same way, with the CFs dissipating the charge. Despite the inherently high electrical conductivity of the CFs, the fact that these are embedded in the matrix limits the conductivity of the pristine CFs, and hence the dissipation effectiveness of the outer CFRP ply is inferior to that of the Cu mesh. For an insulating matrix (E-R) this causes penetration of the CFRP, see Figure 7a. Similar differences in the degree of the inflicted damage between a Cu mesh-protected CFRP specimen and an unprotected specimen, when subjected to a waveform D current pulse with a peak amplitude of 80 kA, have been reported by Kawakami et al.[27] Compared to the G-R test panel, the E-CM-R test panel has the disadvantage that the Cu mesh will need to undergo repair in the strike area to protect against a future lightning strike, whereas the G-R test panel despite its inferior thermal dissipation behavior (see Figure 6) is capable nonetheless, to withstand the electrostatic charges without damage.

The C-scans of the CFRP RIFT test panels without the Cu mesh are presented in Figure 8. The undamaged areas with low signal attenuation are shown in blue, while structural damage gives high attenuation, which is shown in red. For the G-R panel, there is no identifiable damage apart from a couple of red pixels at the strike location, see Figure 8b. Macroscopically, the lightning current caused damage on the E-R and GC-R test panels, which was very similar, with the C-scans showing that the internal damage is slightly greater for the E-R panel than it is for the GC-R panel, see Figure 8a,c. Hence, the C-scan images are in excellent agreement with the findings of the optical examination; see Figure 7a–c.

The images of the CFRP WL test panels after the lightning strike tests are shown in Figure 9. The WL test panels exhibited a slight waviness, which arose from the relatively low pressure applied during the manufacturing process. The WL test panels show more extensive damage compared to their RIFT counterparts. The inferior performance of the WL test panels is attributed to their significantly lower, that is, of two orders of magnitude,

10974628, 2022, 46, Downloaded from https://onlinelibrary.wiley.com/doi/10.1002/app.53157 by Imperial College London, Wiley Online Library on [29/11/2022]. See the Terms and Conditions (https://onlinelibrary.wiley.com/terms-and-conditions) on Wiley Online Library for rules of use; OA articles are governed by the applicable Creative Commons License

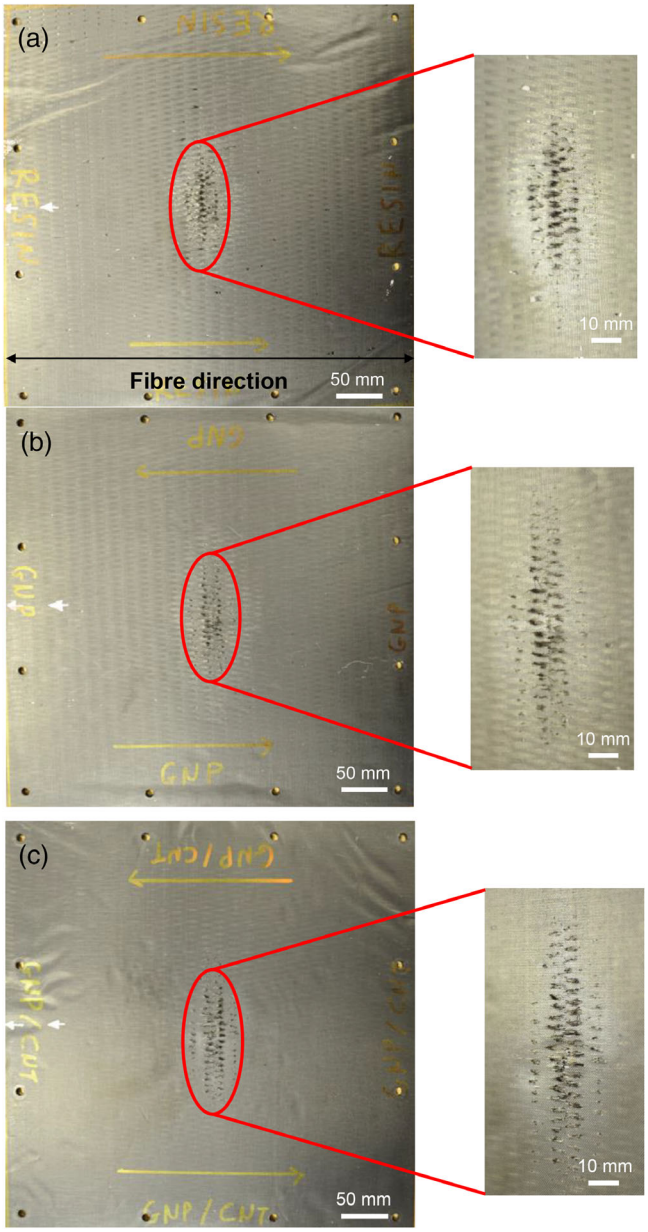


FIGURE 9 Damage of the WL CFRP composite test panels after simulated lightning current tests of 40 kA: (a) epoxy (E-W), (b) 0.5 wt% GNP (G-W) and (c) 0.5 wt% GNP/CNT (GC-W). The magnified region provides a close-up of the damaged area. (Note the yellow arrows indicate the direction of the fibers.) [Color figure can be viewed at wileyonlinelibrary.com]

longitudinal conductivity compared to the RIFT test panels, see Table 3. This has been attributed to the significantly lower carbon-fiber volume fraction of the WL test panels, arising from the limitations of the manufacturing process. The extent of damage is very similar for all the tested test panels, regardless of nanocarbon modification of the matrix. The damage morphology at the strike location shows characteristic signs of abrasion damage, which is visible as broken CFs on the surface as well as matrix pyrolysis. Signs of matrix degradation can be seen in the vicinity of the broken fibers. Despite the extensive damage of the test panels, there are no evident signs of delamination, and any damage appears to be limited to the outer ply. Similar to the CFRP RIFT test panels, the damage predominantly extends perpendicular to the direction of the fibers, that is, from top to bottom in the images in Figure 9. The extent of the damage can be roughly contained within an ellipse, drawn in red in Figure 9, with the length of the major axis being 40 to 60 mm and that of the minor axis being 10 to 20 mm for all three test panels.

Carbon-fiber volume fraction is the dominant factor in dictating the longitudinal conductivity of the CFRP test panels and from examination of the thermal images, see Figure 5, it may be seen that the electrical currents are mainly conducted along the fiber direction for UD panels, as has been reported elsewhere.[45,46] Since a large proportion of the electrical charges is dissipated along the most electrically conductive fiber direction, it is not surprising that the RIFT test panels, having a greater carbon-fiber content, perform considerably better than the WL test panels. Hence, it is not truly valid to compare CFRP laminates with a considerable difference in their carbon-fiber content, and the same comment holds true, of course, not only for electrical properties but also for mechanical properties.

For the RIFT test panels, the addition of GNPs to the epoxy matrix leads to a marginal increase in the electrical conductivity of the transverse direction from 0.052 S/cm for the unmodified panel to 0.074 S/cm, corresponding to an increase of 42%, see Table 3. Although such a small increase in conductivity can hardly explain the improved damage tolerance shown by the G-R panel compared to the E-R, see Figure 7, a lack of correlation between measured 4-probe electrical resistance and the degree of protection offered against lightning has been reported by Rajesh et al.[9] In their work, they reported that CFRP laminates coated with silver-based materials, demonstrating surface conductivities in the order of 10^3 S/cm, exhibited more damage when compared to the unprotected 'baseline' CFRP. Unprotected CFRP laminates with a plain-weave geometry, that is, a [0/ 90] lay-up, similar to that used as the baseline in the study of Rajesh et al., demonstrated a surface conductivity of 16 S/cm.[8] Consequently, it was shown that a conductive coating, with a significant higher surface conductivity compared to the unprotected 'baseline' CFRP of approximately three orders of magnitude higher, did not automatically lead to an improved damage tolerance. This 'disconnect' was attributed to the many interacting parameters governing a lightning strike phenomenon, which cannot be assessed by the normal 4-point probe measurement.

10974628, 2022, 46, Downloaded from https://onlinelibrary.wiley.com/doi/10.1002/app.53157 by Imperial College London, Wiley Online Library on [29/11/2022]. See the Terms and Conditions (https://onlinelibrary.wiley.com/terms-and-conditions) on Wiley Online Library for rules of use; OA articles are governed by the applicable Creative Commons License

This work has further shown that modification of the epoxy matrix with 0.5 wt% of GNPs can emulate the effectiveness of Cu mesh protection, but with a weight reduction for the CFRP structure. Copper has a bulk density of 8.9 g/cm^3,[3] while that of GNPs is only 2.2 g/cm^3.[47] The incorporation of the Cu mesh on top of the CF plies and impregnation of the whole structure, therefore, adds 20% extra weight compared to the unprotected structure, for test panels made via the RIFT process. However, the majority of mass contribution is from the epoxy impregnated into the mesh rather than from the mesh itself, which also greatly reduces the surface conductivity of the pristine Cu mesh. For the Cu mesh used, having a weight of 73 g/m^2 and an open area of 84%, the calculated weight contribution between the epoxy and mesh is 11:1. The Cu mesh used in the present work is one of the lightest meshes on the market, so the use of a heavier Cu mesh in an attempt to reduce the area of mesh damaged during the strike would cause an even greater increase in the weight of the CFRP test panel. Further, the Cu mesh-protected CFRP panel has the additional disadvantage of having to undergo a scarf repair to restore its LSP effectiveness,[27] adding both to maintenance costs and repair times; and potential corrosion problems are an additional concern. On the other hand, the GNP-modified CFRP test panel (G-R) does not require such significant repair, since its structural integrity remained unaffected. Indeed, the GNP-modified CFRP panel is expected to withstand similar currents in the event of a second strike, as its electrical conductivity is not negatively affected by the impact, as confirmed by the post-strike conductivity measurements.

5 | CONCLUSIONS

Lightning strikes can be a serious threat for modern fiber composite aircraft, as they impact each aircraft on average once a year. Without adequate protection, CFRP materials can undergo significant structural damage following a lightning strike due to the poor conductivity characteristics of the composite. The lightning damage resistance of unidirectional (UD) CFRP composite test panels subjected to a simulated lightning test with a current of 40 kA has been examined. Nanocarbon modification of the epoxy matrix of the CFRPs has been explored as a means of improving the electrical properties of the test panels. The CFRP test panels were fabricated using resin-infusion under flexible tooling (RIFT) or by a wet lay-up (WL) process. These two methods produced laminates with a significant difference in their respective fiber volume fractions (V_F), with the RIFT laminates possessing on average a 53% higher V_F compared to the WL laminates. The lightning damage resistance of the CFRP test panels was found to be significantly dependent on their electrical properties, with the conductivity of the longitudinal direction being heavily influenced by the V_F value. Consequently, the WL test panels could not match the lightning strike performance of the RIFT test panels.

The CFRP test panels made by RIFT demonstrated a very good tolerance to lightning currents. In particular, modification of the epoxy matrix with 0.5 wt% of GNPs (G-R) demonstrated a comparable level of protection to the current Cu mesh lightning protection practice. Despite the panel demonstrating a significantly lower electrical conductivity compared to the Cu mesh-protected CFRP, this was not translated to a worse damage tolerance behavior, with both panels demonstrating only surface damage without any penetration occurring. Moreover, the nanocarbon modified panel (a) is significantly lighter than the Cu mesh-protected CFRP panel, (b) does not require to be repaired to protect against a second strike, and (c) does not give rise to any potential corrosion problems. Consequently, modification of thermosetting matrices with conductive nanocarbon fillers is a highly promising route for improving the lightning strike performance of carbon-fiber composites, without adding extra weight. Given the encouraging results of nanocarbon modified CFRP panels for lighting damage resistance, a subject of future studies would be examining the performance under conducted lightning current, by applying the lighting current to a fastener inserted in the panel and observing the current transfer from the fastener to the panel.

AUTHOR CONTRIBUTIONS

Sotirios Kopsidas: Data curation (lead); formal analysis (lead); investigation (lead); writing – original draft (lead). **Ganiu B. Olowojoba:** Conceptualization (lead); investigation (equal); methodology (lead). **Chris Stone:** Methodology (equal). **David Clark:** Methodology (equal); software (lead); writing – review and editing (supporting). **A. Manu Haddad:** Methodology (equal); resources (lead); writing – review and editing (supporting). **Anthony J. Kinloch:** Funding acquisition (lead); investigation (equal); project administration (lead); supervision (lead); writing – review and editing (lead). **Ambrose C. Taylor:** Data curation (equal); formal analysis (equal); investigation (equal); methodology (equal); project administration (lead); resources (lead); supervision (lead); validation (lead); writing – review and editing (lead).

ACKNOWLEDGMENTS

Part of this work was funded by the UK Engineering and Physical Sciences Research Council (EPSRC), Grant

10974628, 2022, 46, Downloaded from https://onlinelibrary.wiley.com/doi/10.1002/app.53157 by Imperial College London, Wiley Online Library on [29/11/2022]. See the Terms and Conditions (https://onlinelibrary.wiley.com/terms-and-conditions) on Wiley Online Library for rules of use; OA articles are governed by the applicable Creative Commons License

Number EP/K016792/1. Dr Sotirios Kopsidas would like to acknowledge the Department of Mechanical Engineering, Imperial College London, UK for funding his PhD studentship. The authors would like to thank Mr Michael Harnos of Dexmet Corporation and Dr Stephan Sprenger of Evonik Industries for supplying the copper mesh and curing agent used in this work. The authors would also like to thank Dr Haibao Liu for conducting the C-scans and Dr Xinying Deng for her help in the manufacture of the CFRP laminates.

DATA AVAILABILITY STATEMENT

The data that support the findings of this study are available from the corresponding author upon reasonable request.

ORCID

Sotirios Kopsidas https://orcid.org/0000-0002-4281-2459
Ganiu B. Olowojoba https://orcid.org/0000-0001-8032-4678
David Clark https://orcid.org/0000-0002-1090-2361
A. Manu Haddad https://orcid.org/0000-0003-4153-6146
Anthony J. Kinloch https://orcid.org/0000-0002-8752-7184
Ambrose C. Taylor https://orcid.org/0000-0003-0863-8423

REFERENCES

[1] C. Soutis, *J. Mater. Sci. Eng. A* **2005**, *412*, 171.
[2] B. Alemour, O. Badran, M. R. Hassan, *J. Aerosp. Technol. Manage.* **2019**, *11*, 1022.
[3] M. Gagné, D. Therriault, *Prog. Aeronaut. Sci.* **2014**, *64*, 1.
[4] B. Zhang, V. R. Patlolla, D. Chiao, D. K. Kalla, H. Misak, R. Asmatulu, *Int. J. Adv. Manuf. Technol.* **2013**, *67*, 1317.
[5] J. H. Lehman, M. Terrones, E. Mansfield, K. E. Hurst, V. Meunier, *Carbon* **2011**, *49*, 2581.
[6] J. Han, H. Zhang, M. Chen, D. Wang, Q. Liu, Q. Wu, Z. Zhang, *Carbon* **2015**, *94*, 101.
[7] Q. Xia, H. Mei, Z. Zhang, Y. Liu, Y. Liu, J. Leng, *Composites, Part B* **2020**, *180*, 107563.
[8] B. Wang, Y. Duan, Z. Xin, X. Yao, D. Abliz, G. Ziegmann, *Compos. Sci. Technol.* **2018**, *158*, 51.
[9] P. Rajesh, F. Sirois, D. Therriault, *Mater. Des.* **2018**, *139*, 45.
[10] Aero Consultants AG, *Dexmet MicroGrid Technical Brochure* **2008** doc. ref. 20080311.
[11] S. Kamiyama, Y. Hirano, T. Okada, T. Ogasawara, *Compos. Sci. Technol.* **2018**, *161*, 107.
[12] Y. Hirano, T. Yokozeki, Y. Ishida, T. Goto, T. Takahashi, D. Qian, S. Ito, T. Ogasawara, M. Ishibashi, *Compos. Sci. Technol.* **2016**, *127*, 1.
[13] T. Yokozeki, T. Goto, T. Takahashi, D. Qian, S. Itou, Y. Hirano, Y. Ishida, M. Ishibashi, T. Ogasawara, *Compos. Sci. Technol.* **2015**, *117*, 277.
[14] Y. J. Lim, D. Carolan, A. C. Taylor, *J. Mater. Sci.* **2016**, *51*, 8631.
[15] T. H. Hsieh, A. J. Kinloch, A. C. Taylor, I. A. Kinloch, *J. Mater. Sci.* **2011**, *46*, 7525.
[16] H. M. Chong, S. J. Hinder, A. C. Taylor, *J. Mater. Sci.* **2016**, *51*, 8764.
[17] E. C. Senis, I. O. Golosnoy, J. M. Dulieu-Barton, O. T. Thomsen, *J. Mater. Sci.* **2019**, *54*, 8955.
[18] K. A. Imran, K. N. Shivakumar, *J. Compos. Mater.* **2019**, *53*, 93.
[19] Y. Li, H. Zhang, H. Porwal, Z. Huang, E. Bilotti, T. Peijs, *Composites, Part A* **2017**, *95*, 229.
[20] E. Logakis, A. A. Skordos, in Proc. ECCM15, Venice, **2012**.
[21] S. Lampkin, W. Lin, M. Rostaghi-Chalaki, K. Yousefpour, Y. Wang, J. Kluss, in Proc. American Society for Composites 34th Technical Conference, Atlanta, September **2019**.
[22] D. K. Chakravarthi, V. N. Khabashesku, R. Vaidyanathan, J. Blaine, S. Yarlagadda, D. Roseman, Q. Zeng, E. V. Barrera, *Adv. Funct. Mater.* **2011**, *21*, 2527.
[23] W. Lin, B. Jony, K. Yousefpour, Y. Wang, C. Park, S. Roy, in Proc. American Society for Composites 35th Technical Conference, Online, September **2020**.
[24] D. G. Papageorgiou, I. A. Kinloch, R. J. Young, *Prog. Mater. Sci.* **2017**, *90*, 75.
[25] S. Kopsidas, G. B. Olowojoba, *J. Appl. Polym. Sci.* **2021**, *138*, 50890.
[26] SAE Aerospace. ARP5412B Aircraft Lightning Environment and Related Test Waveforms, **2013**.
[27] H. Kawakami, P. Feraboli, *Composites, Part A* **2011**, *42*, 1247.
[28] P. Feraboli, M. Miller, *Composites, Part A* **2009**, *40*, 954.
[29] S. Chandrasekaran, C. Seidel, K. Schulte, *Eur. Polym. J.* **2013**, *49*, 3878.
[30] J. Sandler, J. E. Kirk, I. A. Kinloch, M. Shaffer, A. H. Windle, *Polymer* **2003**, *44*, 5893.
[31] J. Li, P. C. Ma, W. S. Chow, C. K. To, B. Z. Tang, J.-K. Kim, *Adv. Funct. Mater.* **2007**, *17*, 3207.
[32] D. Wang, X. Zhang, J.-W. Zha, J. Zhao, Z.-M. Dang, G.-H. Hu, *Polymer* **1916**, *2013*, 54.
[33] L. Yue, G. Pircheraghi, S. A. Monemian, I. Manas-Zloczower, *Carbon* **2014**, *78*, 268.
[34] M. Martin-Gallego, M. M. Bernal, M. Hernandez, R. Verdejo, M. A. Lopez-Manchado, *Eur. Polym. J.* **2013**, *49*, 1347.
[35] E. F. Reia da Costa, A. A. Skordos, I. K. Partridge, A. Rezai, *Composites, Part A* **2012**, *43*, 593.
[36] F. H. Gojny, M. H. Wichmann, B. Fiedler, W. Bauhofer, K. Schulte, *Composites, Part A* **2005**, *36*, 1525.
[37] M. H. Wichmann, J. Sumfleth, F. H. Gojny, M. Quaresimin, B. Fiedler, K. Schulte, *Eng. Fract. Mech.* **2006**, *73*, 2346.
[38] E. Kandare, A. A. Khatibi, S. Yoo, R. Wang, J. Ma, P. Olivier, N. Gleizes, C. H. Wang, *Composites, Part A* **2015**, *69*, 72.
[39] W. Qin, F. Vautard, L. T. Drzal, J. Yu, *Composites, Part B* **2015**, *69*, 335.
[40] ASTM International. ASTM D3171-15 Standard Test Methods for Constituent Content of Composite Materials, **2015**.
[41] I. El Sawi, P. A. Olivier, P. Demont, H. Bougherara, *Compos. Sci. Technol.* **2012**, *73*, 19.
[42] G. B. Olowojoba, S. Kopsidas, S. Eslava, E. S. Gutierrez, A. J. Kinloch, C. Mattevi, V. G. Rocha, A. C. Taylor, *J. Mater. Sci.* **2017**, *52*, 7323.

10974628, 2022, 46, Downloaded from https://onlinelibrary.wiley.com/doi/10.1002/app.53157 by Imperial College London, Wiley Online Library on [29/11/2022]. See the Terms and Conditions (https://onlinelibrary.wiley.com/terms-and-conditions) on Wiley Online Library for rules of use; OA articles are governed by the applicable Creative Commons License

[43] A. G. Duba, *Fuel* **1977**, *56*, 441.
[44] X. Hu, Y. Mai, *Compos. Sci. Technol.* **1993**, *46*, 147.
[45] F. S. Wang, Y. Y. Ji, X. S. Yu, H. Chen, Z. F. Yue, *Compos. Struct.* **2016**, *145*, 226.
[46] F. Wang, X. Ma, Y. Zhang, S. Jia, *Appl. Sci.* **2018**, *8*, 1791.
[47] R. B. Ladani, S. Wu, A. J. Kinloch, K. Ghorbani, J. Zhang, A. P. Mouritz, C. H. Wang, *Mater. Des.* **2016**, *94*, 554.

How to cite this article: S. Kopsidas, G. B. Olowojoba, C. Stone, D. Clark, A. M. Haddad, A. J. Kinloch, A. C. Taylor, *J. Appl. Polym. Sci.* **2022**, *139*(46), e53157. https://doi.org/10.1002/app.53157

10974628, 2022, 46, Downloaded from https://onlinelibrary.wiley.com/doi/10.1002/app.53157 by Imperial College London, Wiley Online Library on [29/11/2022]. See the Terms and Conditions (https://onlinelibrary.wiley.com/terms-and-conditions) on Wiley Online Library for rules of use; OA articles are governed by the applicable Creative Commons License